Journal of Inorganic Biochemistry 201 (2019) 110806

Contents lists available at ScienceDirect

Journal of Inorganic Biochemistry

journal homepage: www.elsevier.com/locate/jinorgbio

Structural insights for vanadium catecholates and iron-sulfur clusters obtained from multiple data analysis methods applied to electron spin relaxation data

Thacien Ngendahimana, Richard Ayikpoe, John A. Latham, Gareth R. Eaton, Sandra S. Eaton*

Department of Chemistry and Biochemistry, University of Denver, Denver, CO 80210, United States of America.

ARTICLE INFO

Keywords:
Iron-sulfur clusters
Hydrogenase maturase
Mycofactocin maturase
Distribution of exponentials
Pyruvate formate lyase activating enzyme
Vanadium(IV) catecholate

ABSTRACT

Electron paramagnetic resonance (EPR) inversion recovery curves for vanadium catecholates and iron-sulfur clusters were analyzed with three models: the sum of two exponentials, a stretched exponential, and a model-free distribution of exponentials (UPEN). For all data sets studied fits with a stretched exponential were statistically indistinguishable from the sum of two exponentials, and were significantly better than for single exponentials. UPEN provides insights into the structures of the distributions. For a vanadium(IV) tris catecholate the distribution of relaxation rates calculated with UPEN shows the contribution from spectral diffusion at low temperatures. The energy of the local mode for this complex, found from the temperature dependence of the spin lattice relaxation, is consistent with values expected for a metal-ligand vibration. For the $[2Fe\text{-}2S]^{+}$ cluster in pyruvate formate lyase activating enzyme (PFL-AE) the small stretched exponential β values (0.3) at low temperature and the distributions calculated with UPEN reflect the contribution from a second rapidly relaxing species that could be difficult to detect by continuous wave EPR. The distributions in $1/T_1$ for the $[4Fe\text{-}4S]^{+}$ clusters in Mycofactocin maturase were about a factor of four wider than for the three other systems studied. The very broad distribution of relaxation rates may be due to protein mobility and distributions in electronic energies and local environments for the clusters. UPEN provides insight into several situations that can result in low values of stretch parameter β including contributions from spectral diffusion, overlapping signals from distinguishable clusters, or very wide distributions.

1. Introduction

Analysis of the temperature dependence of electron spin lattice relaxation rates ($1/T_1$) for transition metal complexes can provide important insights into electronic structure and local environment [1]. Distributions in *g* and nuclear hyperfine *A* values, that have been denoted as *g*-strain and *A*-strain have been characterized for metal complexes including Cu(II) [2] and iron-sulfur clusters [3,4]. Since relaxation processes involve modulation of spin-orbit coupling, and spin-orbit coupling generates deviations from the free electron *g*-value, it is likely that *g*-strain can result in a distribution of relaxation rates. There also is strong evidence for distributions in zero field splittings [5] that can lead to distributions of relaxation rates. Thus, there are important incentives for analyzing relaxation data with models for distributions. Also, for certain situations there are models that predict multiple contributions to inversion recovery curves. For example, there may be contributions from cross relaxation or spectral diffusion, in addition to spin lattice relaxation. Multiple species with overlapping electron paramagnetic resonance (EPR) signals also could result in distinguishable contributions to relaxation. Accurate analysis of the experimental data is needed to provide the most precise values for structural characterization and analysis of the temperature dependence of relaxation. A crucial issue then is how to distinguish between distributions of exponentials and sums of discrete contributions when analyzing experimental inversion recovery data.

The most widely used pulse EPR technique for measuring T_1 is inversion recovery [1]. Inversion recovery data typically are analyzed by only one of the models discussed in the methods section. In this paper, we compare the time constant obtained by multiple methods. We are particularly interested in comparison of the results for distributions that are obtained from stretched exponentials and a model-free analysis of distributions of relaxation times that is designated as UPEN (uniform penalty inversion of multiexponential decay data) [6,7]. We seek to evaluate ways to recognize cases in which there is more than one

* Corresponding author.
E-mail address: sandra.eaton@du.edu (S.S. Eaton).

https://doi.org/10.1016/j.jinorgbio.2019.110806
Received 14 May 2019; Received in revised form 6 August 2019; Accepted 21 August 2019
Available online 02 September 2019
0162-0134/

distinguishable contribution to relaxation, to characterize the structures of the distributions and to use that information to reveal properties of the metal centers. We examined the relaxation of vanadium catecholates, a class of compounds that has recently been found to have anticancer properties rivaling cisplatin [8–10]. Vanadium catecholates also are model systems for qubits [11]. Data for vanadium(IV) tris catecholate ($(n\text{-}Bu_3NH)_2$ $[V(C_6H_4O_2)_3]$)($V(cat)_3^{2-}$) [11] were selected as an example of this class of compounds. Iron-sulfur clusters are the redox active centers in a wide range of metalloenzymes. The temperature dependence of spin-lattice relaxation for iron-sulfur clusters can be used to determine the energies of low-lying excited states [12], and characterize interactions between neighboring clusters [13]. We analyzed the inversion recovery curves for the $[2Fe\text{-}2S]^+$ cluster in pyruvate formate lyase activating enzyme (PFL-AE) [13], the $[2Fe\text{-}2S]^+$ cluster in hydrogenase maturase F (HydF) [13], and the $[4Fe\text{-}4S]^+$ clusters in the radical S-adenosylmethionine protein mycofactocin maturase, MftC.

2. Materials and methods

Samples of MftC were prepared as previously reported [14]. Solutions for EPR studies were prepared in a Coy inert atmosphere chamber, transferred into 4 mm OD quartz tubes and flash frozen in liquid nitrogen. Tubes were temporarily capped with clamped tygon tubing, removed from the chamber, partially evacuated, and flame sealed. Samples were stored in liquid nitrogen and inserted frozen into the precooled resonator. Inversion recovery data were acquired on a Bruker E580 spectrometer using a split ring resonator, an Oxford CF935 cryostat, and a Bruker/ColdEdge Stinger closer-cycle cryogenic system. Inversion recovery data were acquired using a π - t - $\pi/2$ - τ - π - τ - echo sequence in which t is varied and τ is constant, with a $\pi/2$ pulse length of 16 ns. The inversion recovery data that are the primary focus of this study were collected at the maximum in the field-swept echo detected spectrum ($g_y = 1.931$) because the signal to noise ratio is better at this position. In addition, inversion recovery data were acquired at three other positions in the spectrum (g_x, g_z, and intermediate between g_y and g_z) to test for orientation dependence of relaxation and of distribution widths. Tests for orientation dependence are important for the interpretation of distributions. If the relaxation times are orientation dependent, contributions to the inversion recovery data from orientations with different relaxation times would result in a distribution of values.

2.1. Data analysis models

Often inversion recovery curves are not well fit with a single exponential (Eq. (1)).

$$Y(t) = C_0 + C_1\, e^{-t/T_1} \tag{1}$$

where C_0 is the constant offset, C_1 is the scaling factor, and T_1 is the spin lattice relaxation time. Although a single-parameter fit is convenient for analysis of temperature dependence, it may mask key features of the species studied.

When the signal-to-noise is sufficiently high, it may be possible to argue statistically that the fit to the data is better for the sum of two exponentials (Eq. (2)) than for a single exponential [15–18].

$$Y(t) = C_0 + C_1\, e^{-t/T_1(long)} + C_2\, e^{-t/T_1(short)} \tag{2}$$

where C_2/C_1 is the ratio of the contributions from relaxation processes with time constants $T_1(short)$ and $T_1(long)$. However, there often is significantly greater scatter in the fit parameters for the sum of two exponentials than for a single exponential, which can complicate the analysis of temperature dependence. In addition, a better fit to a sum of two exponentials than to one exponential could be a surrogate for a distribution of exponentials, which is not easy to distinguish statistically [18].

The stretched exponential function (Eq. (3)) has been used to analyze distributions of exponentials for T_1 in solid state nuclear magnetic resonance (NMR) [19–21], in rigid lattice EPR [22–26], and for spin-labeled lipids in eye lenses [27].

$$Y(t) = C_0 + C_1 e^{\left(-t/T_{1mp}\right)^{\beta}} \tag{3}$$

where T_{1mp} is the most probable value in the distribution and β is the stretch parameter [19]. A β of 1 corresponds to an infinitely narrow distribution and β approaching 0 would be an infinitely wide distribution. The essential physics of the system is represented by the probability density function for the distribution of exponentials. Spin echo dephasing is an example of a system in which the processes that drive dephasing have been analyzed in detail which provides the basis for interpreting values of the stretch parameter to distinguish between domination by nuclear spin diffusion ($\beta \sim 2$) from instantaneous diffusion ($\beta \sim 1$) or motional averaging that is fast on the experimental timescale ($\beta < 1$) [28,29]. However, if the physics of the system has not been built into the function, there is no physical significance of the derived value of β.

Eq. (4) can be used to calculate the average value for a distribution that was analyzed with a stretched exponential [19].

$$T_{1avg} = \frac{T_{1mp}}{\beta}\Gamma\left(\frac{1}{\beta}\right) \tag{4}$$

where Γ is the mathematical gamma function.

Within a set of data, if β is weakly temperature dependent, the temperature dependence of T_{1mp} and T_{1avg} are similar. However, if β is temperature dependent, the analysis of the temperature dependence of T_{1mp} and T_{1avg} may be sufficiently different that one might draw different conclusions about the mechanism of relaxation. The calculation of T_{1avg} has the advantage that the temperature dependence of β is included, so this is the value from the stretched exponential analysis that is used in the comparisons in this paper.

The stretched exponential fit (Eq. 3) is based on a Kohlrausch-Williams-Watts distribution function [19], which may not be appropriate for T_1 for some transition metal complexes. The UPEN method is an alternate approach to characterizing distributions of exponentials, Eq. (5) [6,7]. Instead of starting with an *a priori* model of the distribution, the UPEN algorithm starts with a sum of exponentials and searches for the set of coefficients that give the best fit to the experimental data.

$$Y(t) = C_0 + \sum_{k=1}^{M} p_k\, e^{-t/T_k} \tag{5}$$

where M is the number of exponentials that are summed (typically 100) and p_k is the relative probability within the distribution for time constant T_k. The software also calculates the geometric mean for the distribution. The integral of the probability distribution permits calculation of the ratios of populations of species with relaxation rates in specific segments of the distribution.

Eq. (6) has been proposed to separate the contribution to inversion recovery curves for triarylmethyl radicals due to cross relaxation from that of spin lattice relaxation.

$$Y(t) = C_0 + C_1\left[e^{-t/T_1 + \sqrt{\frac{t}{q}}}\right] \tag{6}$$

where the term in $\sqrt{t/q}$ reflects the contribution from cross relaxation [30].

2.2. Data analysis

Signal-to-noise was calculated as the ratio of the signal amplitude (maximum minus minimum) to the root mean square noise in the final 20% of the data array. Fitting of the data with the sum of two

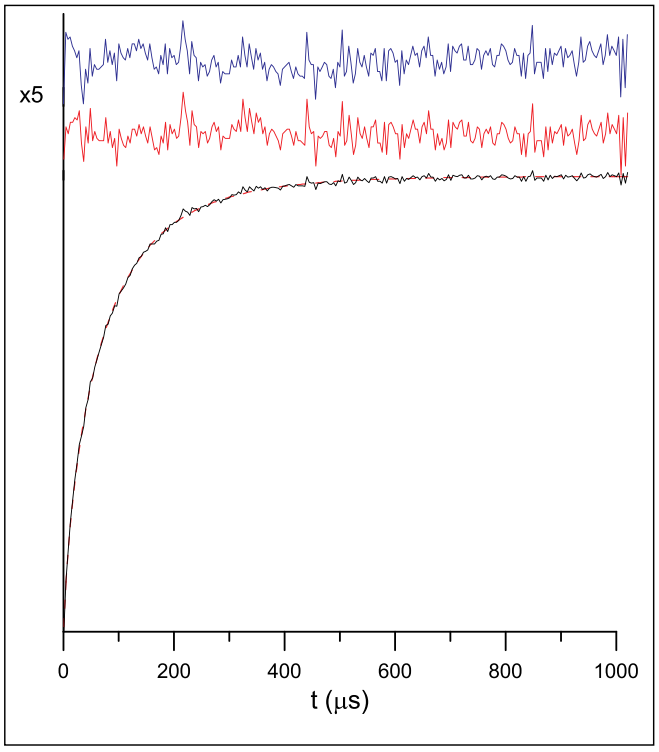

Fig. 1. Comparison of fits to inversion recovery data for the $[2Fe\text{-}2S]^{+}$ in PFL-AE at 30 K.
(black solid line), experimental data; (- - -) fit to the data with a stretched exponential, T_1 = 66 μs, β = 0.75; (solid red line), residuals for fit with stretched exponential; (solid blue line), residuals for fit to two exponentials with T_1 = 105 and 20 μs. (For interpretation of the references to colour in this figure legend, the reader is referred to the web version of this article.)

exponentials (Eq. 2) or a stretched exponential was performed with the Bruker E580 software. Fitting with UPEN was performed with a local version [31] of the software provided by R. J. S. Brown [6,7]. The shortest and longest values of T_1 that are included in the UPEN probability distributions are determined by the shortest and longest times at which the inversion recovery data were recorded. The y axes of the UPEN plots are in arbitrary units. The fits of the data for $V(cat)_3^{2-}$ with Eq. (6) were reported previously [11].

3. Results and discussion

For the inversion recovery data examined in this report the quality of the fits of the data with the sum of two exponentials were statistically indistinguishable from fits with a stretched exponential. An example of the quality of the fits is shown in Fig. 1. The fit line that is shown in the figure is for a stretched exponential, and both were significantly better than for single exponentials. The deviations between the experimental data and the fit lines are much less than the noise in the data. In the following discussion we show that unless there is a second contribution with a substantially different relaxation, the relaxation times obtained for the means of distributions fall between the limits defined by the long and short components obtained in a two component fit. Unless there is a physical model for a particular system that predicts two contributions, our results suggest that it would be wiser to analyze data in terms of a distribution rather than two exponentials. If there are, in fact, two distinguishable contributions this is revealed by a UPEN analysis without assuming this to be the case in advance.

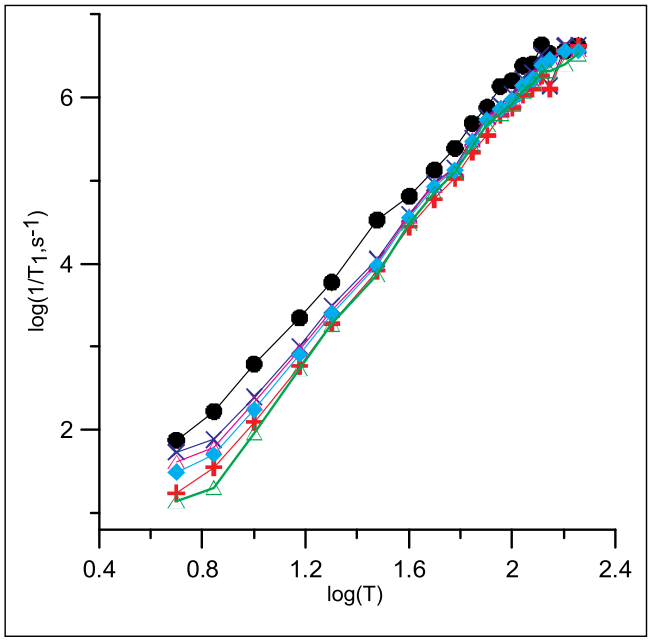

Fig. 2. Temperature dependence of spin lattice relaxation rates for $V(cat)_3^{2-}$ obtained from the same inversion recovery data using (•) Eq. (2) short component, (+) Eq.(2) long component, (△) stretched exponential Eq. (3), (♦) stretched exponential Eq. (4), (X) Eq. (5) UPEN geometric mean, and (△) Eq. (6).

3.1. $V(cat)_3^{2-}$

For $V(cat)_3^{2-}$, it was reported previously that the fits to the inversion recovery curves were better with Eq. (6), which includes a contribution from cross relaxation, than with a single exponential (Eq. (1)) below 40–50 K, although the opposite is true at higher temperatures [11]. To avoid the problems of two different fitting regimes, the data in Ref. [11] were fit with Eq. (6) over the full temperature range of 5 to 160 K. The cross relaxation term in Eq. (6) is not negligible in the temperature range of 5 to 40 K. Contributions from cross relaxation or spectral diffusion frequently are observed in inversion recovery curves [13,14]. Values of T_1 obtained with Eqs. (3) to (5) fall between the limits set by the long and short components of the two component fit calculated with Eq. (2) (Fig. 2). The geometric mean of T_1 calculated from the UPEN distribution is similar to the values of T_1 calculated for a stretched exponential with either Eq. (3) for the most probable value or Eq. (4) for the average value, demonstrating that the methods are consistent. Values of T_1 from Eq. (6) are similar to values from the stretched exponential and UPEN analyses above about 25 K, but are longer at lower temperatures, suggesting that the contributions from cross relaxation that are explicitly taken into account with Eq. (6) impact the averages calculated with other analyses. Above 80 K the value of β is approximately constant at about 0.9 (Fig. 3), and the relatively large value of β indicates that the distribution is narrow. Below 80 K the value of β decreases, becoming 0.73 at 10 K. Since the values of β vary only from 0.73 to 0.9 the temperature dependence of T_1 calculated using Eq. (3) and (4) are similar (Fig. 2). The temperature dependence of the UPEN probability distributions (Eq. (5) and Fig. 4) provide insight into the temperature dependence of β (Fig. 3). The probability distribution shifts to higher rates with increasing temperature consistent with the temperature dependence of rates shown in Fig. 2. The widths of the distributions of relaxation rates for $V(cat)_3^{2-}$ are weakly temperature dependent above about 70 K (data not shown). The apparently narrow distribution at 160 K, located at the rapid rate extreme of the plot, reflects the fact that some components of the relaxation time

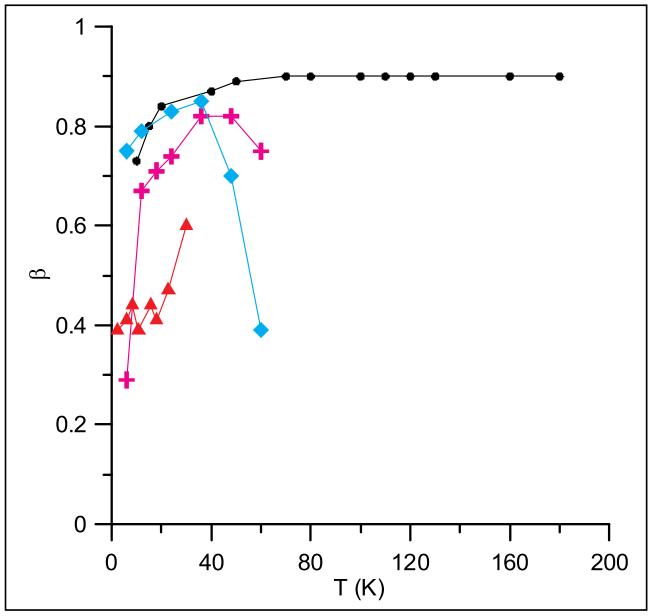

Fig. 3. Temperature dependence of stretch parameter, β Eq. (3), for fits to inversion recovery data for (•) $V(cat)_3^{2-}$, (+) $[2Fe\text{-}2S]^+$ in PFL-AE, (♦) $[2Fe\text{-}2S]^+$ in HydF, and (▲) $[4Fe\text{-}4S]^+$ in MftC.

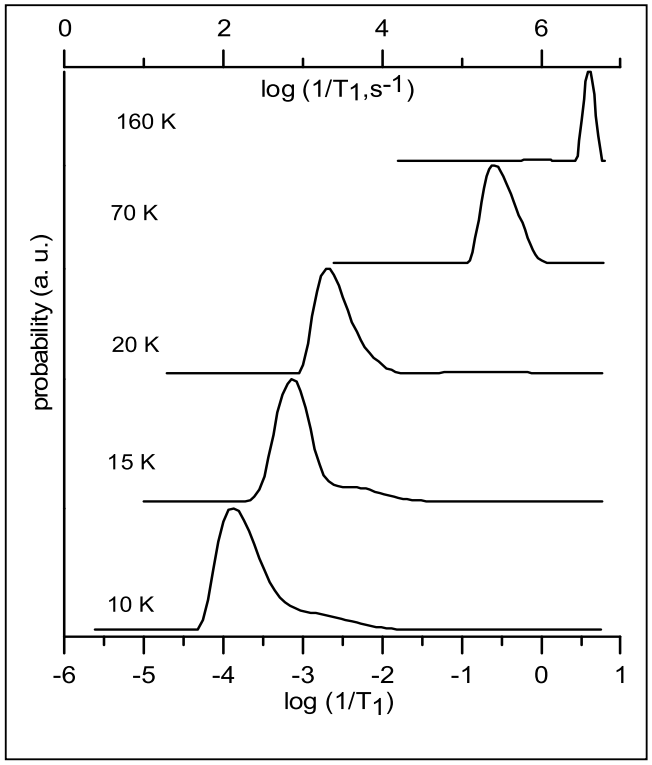

Fig. 4. Examples of the probability distributions for $1/T_1$ of $V(cat)_3^{2-}$ calculated with UPEN (Eq. 5) at selected temperatures. The lower x axis is based on T_1 in μs for which $\log(1/T_1) = 0$ corresponds to $T_1 = 1$ μs. The upper axis has T_1 in s, which are the units for the y axis of Fig. 2. The very narrow distribution at 160 K results from the fact that at this temperature some components of the distribution are short relative to the deadtime of the resonator.

distribution at this temperature are short relative to the resonator deadtime and these components are not adequately represented in the data. As temperature is decreased below about 20 K a second component is increasingly prominent in the UPEN distributions (Fig. 4). The observation of a second component in the distributions at lower temperatures is consistent with the previously reported observation that below about 40 K the fits to the inversion recovery data were better for Eq. (6), which includes a contribution from cross relaxation than for a single exponential (Eq. (1)) [11]. The integrated intensity of the probability for the second (faster relaxing) component at 10 K is about 10% of the total probability.

Stretched exponentials have been used previously to fit inversion recovery curves for V(IV) complexes. Reported values of β as a function of temperature include 0.6 (5 K) to 0.8 (300 K) for vanadyl phthalocyanine doped into titanyl phthalocyanine [32], 0.6 (10 K) to 0.9 (110 K) for vanadyl bis(dipivaloylmethane) in toluene:CH_2Cl_2, 0.3 (5 K) to ~1 (100 K) for vanadyl catecholates in 3:1 CH_2Cl_2: benzene [25], 0.43 (10 K) to 1.03 (150 K) for vanadyl dithiolates doped into diamagnetic Mo═O analogs [33], and 0.5 (5 K) to 0.7 (200 K) for tetrahedral V(IV) alkoxides diluted into the Ti(IV) analog [23]. The pattern for these various V(IV) complexes is increasing β with increasing temperature, which had not been interpreted. For $V(cat)_3^{2-}$ comparison of the temperature dependence of β with the UPEN plots suggests that increasing contributions from spectral diffusion or cross relaxation at lower temperatures can explain the temperature dependence of β that has been reported previously for other V(IV) complexes, without explanation. We propose that when substantially lower values of β are observed at lower temperatures, data should also be analyzed with UPEN to determine whether there are multiple contributions to relaxation at lower temperatures that could arise from spectral diffusion.

A goal of many studies of the temperature dependence of T_1 is determination of the dominant relaxation processes. A key question is whether various methods of analyzing the inversion recovery curves change the values of T_1 sufficiently that it impacts the interpretation of the relaxation mechanism. For example, to take account of contributions from spectral diffusion is it necessary to use Eq. (6) or are the fits to a stretched exponential (Eq. (4)) sufficient? The relaxation times for $V(cat)_3^{2-}$ obtained from the inversion recovery curves with Eq. (4) or Eq. (6) were modeled with the sum of contributions from the direct, Raman, and local mode processes (Eq. (7)). The modeling results are shown in Fig. 5 and the fitting parameters are summarized in Table 1.

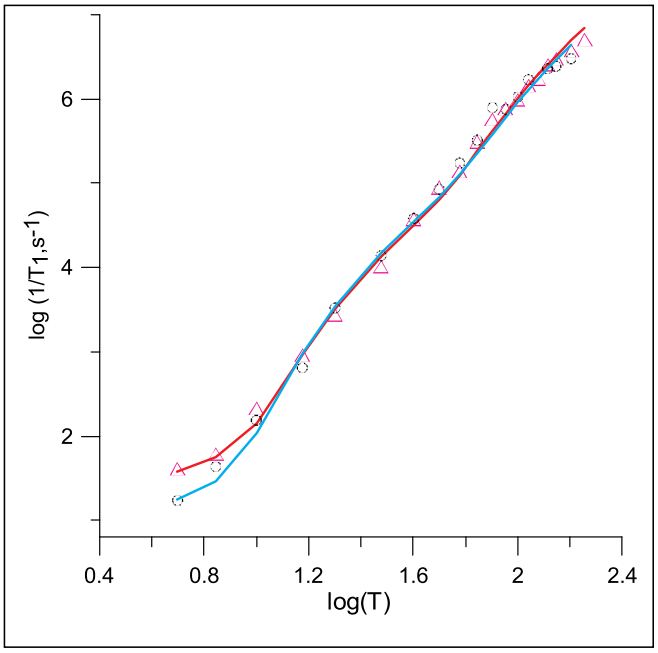

Fig. 5. Temperature dependence of $1/T_1$ for $V(cat)_3^{2-}$ for values calculated from the same inversion recovery curves with (i) (△) stretched exponential Eq. 3 or (ii) **(O)** with Eq. 6. The solid lines are the fits to the sum of contributions from direct, Raman, and local mode process with parameters summarized in Table 1.

Table 1
Parameters obtained by fitting the temperature dependence of $1/T_1$ with Eq. (7).

Fitting method for inversion recovery data	A_{dir} $s^{-1}K^{-1}$	A_{Ram} s^{-1}	θ_D K	A_{loc} s^{-1}	Δ_{loc} K
Eq. (6)[a]	3.5	1.9×10^6	95	5.0×10^7	440
Eq. (4)	7.5	1.7×10^6	95	5.4×10^7	430

[a] Values of q for the fits with Eq. (6) are listed in the Supplementary Information for Ref. [11].

The primary difference in the modeling parameters is that the coefficient for the direct process, which is $3.5\,s^{-1}K^{-1}$ when the inversion recovery curves are fit with Eq. (6) increases to $7.5\,s^{-1}K^{-1}$ when the recovery curves are fit with the stretched exponential (Eq. (4)). Thus, for this data set, the fitting to analyze the mechanisms of relaxation (Eq. (7)) distinguished the characteristic weak temperature dependence of the direct process even when the fitting to individual inversion recovery curves at low temperature did not separate that contribution. The designation of 'direct process' is used here to denote all processes with approximately linear dependence of $1/T_1$ on T, which may include cross relaxation and spectral diffusion.

$$\frac{1}{T_1} = A_{dir}T + A_{Ram}\left(\frac{T}{\theta_D}\right)^9 J_8\left(\frac{\theta_D}{T}\right) + A_{loc}\left[\frac{e^{\Delta_{loc}/T}}{\left(e^{\Delta_{loc}/T}-1\right)^2}\right] \quad (7)$$

where J_8 is the transport integral that is described by Eq. (8)

$$J_8\left(\frac{\theta_D}{T}\right) = \int_0^{\theta_D/T} x^8 \frac{e^x}{(e^x-1)^2}dx \quad (8)$$

and A_{dir} = coefficient of the direct process, A_{Ram} = coefficient of the Raman process.

θ_D = Debye temperature, A_{loc} = Coefficient of the local mode, and Δ_{loc} = Energy of the local mode processes.

The Debye temperature of 95 K (Table 1) is in a range that is typical for glassy matrices [1,34]. For trityl radicals that are used for *in vivo* oximetry the energy of the local mode matched with infrared vibrational frequencies that are tentatively assigned as C-S vibrations, so it was proposed that these modes play a significant role in spin lattice relaxation [35]. The energy of the local mode for $V(cat)_3^{2-}$, 430–440 K, corresponds to about $305\,cm^{-1}$. Vibrational spectra of $V(cat)_3^{2-}$ at frequencies below $500\,cm^{-1}$ have not been recorded. However, in the infrared spectra of vanadyl bis(acetylacetonate) [36] and vanadyl bis(β-diketophenol) [37] there are bands at $369\,cm^{-1}$ and $380\,cm^{-1}$, respectively, that are assigned to V—O (single bond) stretches. Based on the similarity between the $305\,cm^{-1}$ energy of the local mode calculated from the EPR relaxation times of $V(cat)_3^{2-}$ and the energies of V—O stretches for other V(IV) complexes, it is proposed that the V—O (single bond) stretch makes significant contributions to the electron spin relaxation for $V(cat)_3^{2-}$.

3.2. [2Fe-2S]$^+$ in PFL-AE

In the original report the temperature dependence of $1/T_1$ for [2Fe-2S]$^+$ in PFL-AE was based on single exponential fits to inversion recovery data [13]. The values of $1/T_1$ obtained for these data using Eqs. (2) to (5) are compared in Fig. 6. Except at 15 K, the relaxation rates calculated using Eqs. (3)–(5) fall within the range defined by the long and short components of the fit with Eq. (2). The values of stretch parameter β are about 0.7 to 0.8 at 20 to 60 K (Fig. 3) but fall to 0.3 at 15 K. Because of the smaller value of β at 15 K, the 'most probable' value of $1/T_1$ calculated with Eq. (3) is significantly different from the 'average' value of $1/T_1$ calculated with Eq. (4). The average value of $1/T_1$ calculated using Eq. (4) is more similar to values of $1/T_1$ calculated

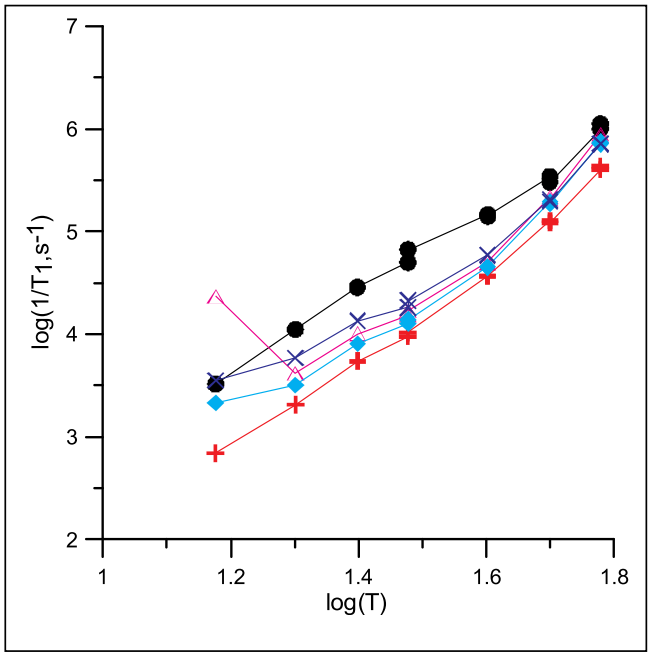

Fig. 6. Temperature dependence of spin lattice relaxation rates for [2Fe-2S]$^+$ in PFL-AE obtained from inversion recovery data using (•) Eq. (2) short component, (+) Eq. (2) long component, (△) stretched exponential Eq. (3), (♦) stretched exponential Eq. (4), and (X) Eq. (5) UPEN geometric mean.

by other methods of data analysis than the value calculated with Eq. (3). The temperature dependence of the UPEN distributions (Eq. (5), Fig. 7) shows that at 15 K there is a large additional contribution from a faster relaxing species. The inversion recovery data were acquired at a magnetic field that corresponds to the maximum in the field-swept echo-detected absorption curve for the [2Fe-2S]$^+$ cluster [13]. The continuous wave (CW) EPR spectra for the PFL-AE sample show that at the magnetic field where the inversion recovery data were acquired there is an overlapping contribution from a faster relaxing [3Fe-4S]$^+$ cluster that becomes observable only at lower temperatures. The contribution to the inversion recovery curves from the [3Fe-4S]$^+$ cluster are negligible at higher temperatures, but are detectable at 30 K and significant at 15 K. For this sample, the decrease in the value of β below 20 K is an indicator that there is an additional contribution to the inversion recovery data. The integral of the probability distribution at 15 K (Fig. 7) has 40% of the probability assigned to the slower relaxing [2Fe-2S]$^+$ cluster and 60% to the faster relaxing [3Fe-4S]$^+$ cluster. Since the signals for the two clusters are extensively overlapped in the CW spectrum this estimate of speciation would be difficult to ascertain from the CW spectrum [13].

Analysis of these data demonstrate that the temperature dependence of β may indicate significant contributions from a second species with distinguishable relaxation rates, such as the [3Fe-4S]$^+$ cluster in PFL-AE, which can be confirmed by analysis with UPEN. Integration of the areas under sections of the distribution permits quantitation of the concentrations of species.

3.3. [2Fe-2S]$^+$ in HydF

In the original report the temperature dependence of $1/T_1$ for [2Fe-2S]$^+$ in HydF was based on single exponential fits to the inversion recovery curves [13]. The temperature dependence of $1/T_1$ obtained from these data using Eqs. (2) to (5) is compared in Fig. 8. The signal-to-noise at 15, 50 and 60 K for the inversion recovery data for this sample is < 50, which may contribute to greater uncertainty in the values of the short component calculated with Eq. (2) than for the prior data sets for which the signal-to-noise was above 100. Except at the lowest and

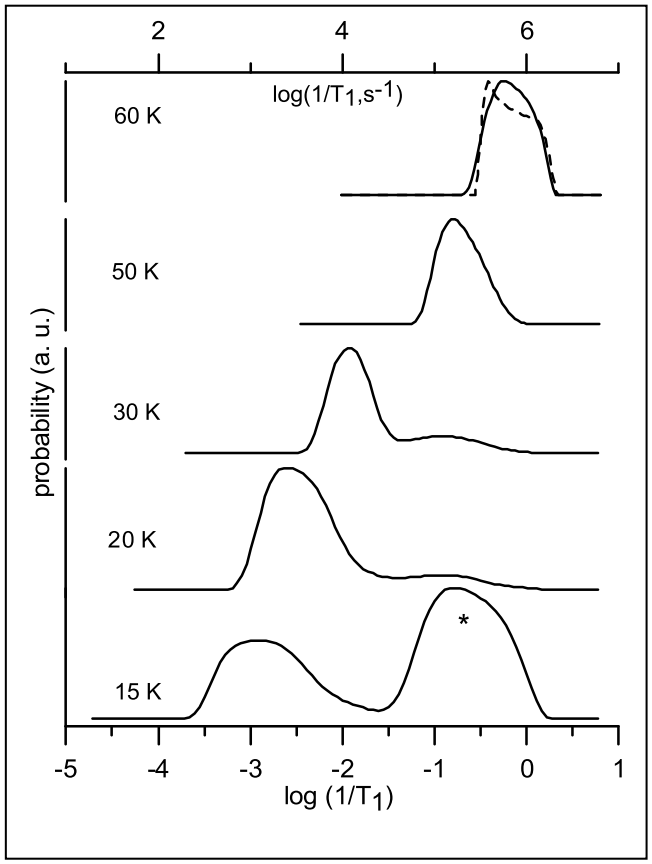

Fig. 7. Examples of the probability distributions for $1/T_1$ of $[2Fe\text{-}2S]^+$ in PFL-AE calculated with UPEN (Eq. (5)) at selected temperatures. The lower x axis is based on T_1 in μs for which $\log(1/T_1) = 0$ corresponds to $T_1 = 1$ μs. The upper axis has T_1 in s, which are the units for the y axis of Fig. 6. The dashed line at 60 K is the distribution that is obtained when a 5-point smooth is applied to the original data, prior to analysis with Eq. (5). The probabilities marked with * are attributed to an overlapping signal from an $[3Fe\text{-}4S]^+$ cluster that contributes to the inversion recovery curves only at lower temperatures.

highest temperatures, the values of T_1 obtained by fitting with Eqs. (3) to (5) are within the limits defined by the long and short components calculated with Eq. (2). The values of T_1 calculated as the geometric mean in UPEN (Eq. (5)) are similar to the average values from the stretch exponential fit calculated with Eq. (4). The values of β are in the range of 0.75 to 0.85 at 15 to 40 K (Fig. 3) but fall to 0.7 and 0.4 at 50 and 60 K, respectively. The UPEN plots (Fig. 9) also show broader distributions at 50 and 60 K. The smaller values of β, and broader UPEN distributions at 50 and 60 K are attributed to the lower signal-to-noise than at lower temperatures.

3.4. $[4Fe\text{-}4S]^+$ in MftC

In MftC there are overlapping signals from three $[4Fe\text{-}4S]^+$ clusters [14]. The *g* values of the three clusters are similar, so the EPR signals overlap extensively. The temperature dependence of the $1/T_1$ values obtained by analysis of the inversion recovery curves at $g_y = 1.931$ for the $[4Fe\text{-}4S]^+$ clusters in MftC using Eqs. (2) to (5) are compared in Fig. 10. Values of T_1 calculated by Eqs. (3) to (5) are similar. The ratio of the T_1 values for the long and short components calculated using Eq. (2) is 15 to 20 for MftC, which is much larger than the ratios of 2 to 5 that were found for the three other paramagnetic centers examined. When the distribution widths are this large it is difficult to select data acquisition windows that adequately sample all components of the distributions, which may contribute to the deviation from monotonic

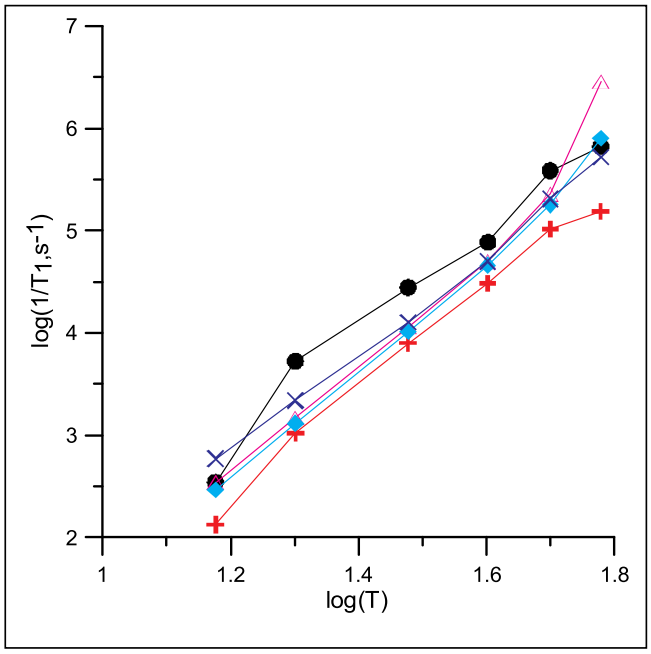

Fig. 8. Temperature dependence of spin lattice relaxation rates for $[2Fe\text{-}2S]^+$ in HydF obtained from inversion recovery data using (•) Eq. (2) short component, (+) Eq. (2) long component, (△) stretched exponential Eq. (3), (♦) stretched exponential Eq. (4), and (χ) Eq. (5) UPEN geometric mean.

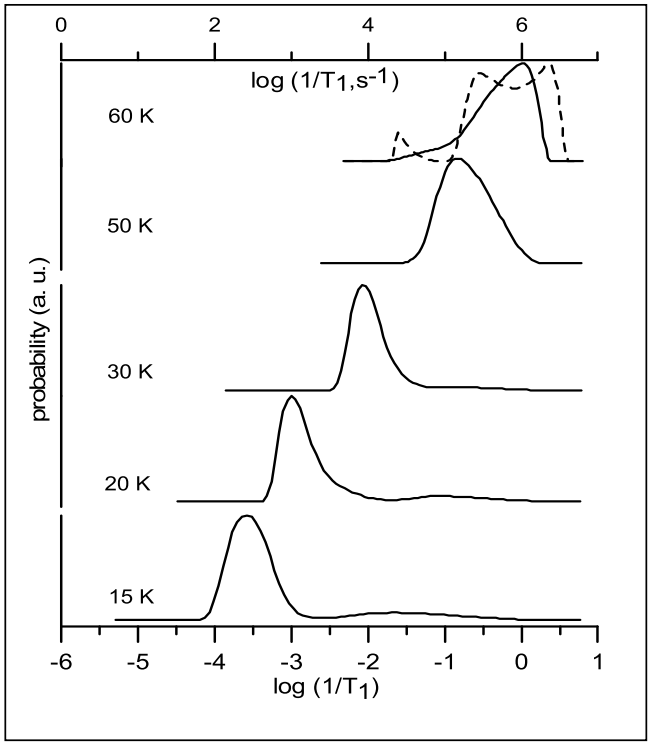

Fig. 9. Examples of the probability distributions for $1/T_1$ of $[2Fe\text{-}2S]^+$ in HydF calculated with UPEN (Eq. 5) at selected temperatures. The lower x axis is based on T_1 in μs for which $\log(1/T_1) = 0$ corresponds to $T_1 = 1$ μs. The upper axis has T_1 in s, which are the units for the y axis of Fig. 8. The dashed line at 60 K is the distribution that is obtained when a 5-point smooth is applied to the original data, prior to analysis with Eq. (5).

behavior in the temperature dependence of $1/T_1$ (Fig. 10). The large widths of the distributions are also reflected in low β values of about 0.4 (Fig. 3) and very broad UPEN distributions (Fig. 11). Inversion recovery

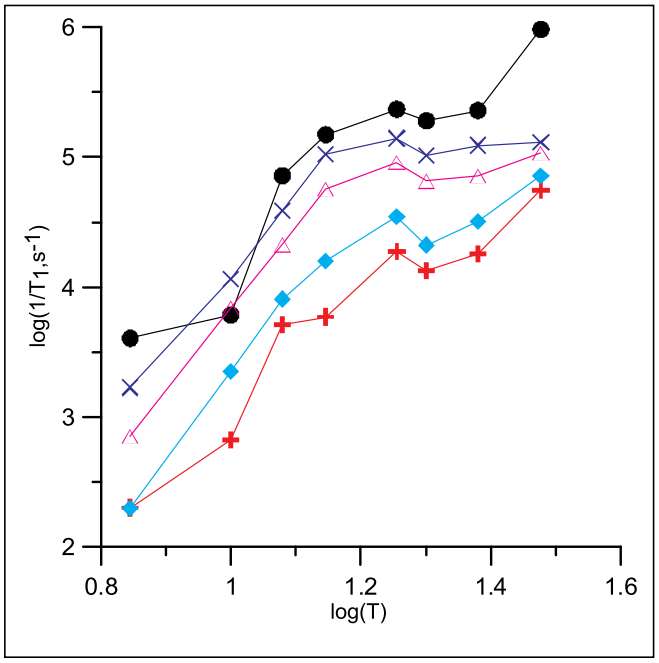

Fig. 10. Temperature dependence of spin lattice relaxation rates for $[4Fe\text{-}4S]^{+}$ in MftC obtained from inversion recovery data using (•) Eq. (2) short component, (+) Eq. (2) long component, (△) stretched exponential Eq. (3), (♦) stretched exponential Eq. (4), and (X) Eq. (5) UPEN geometric mean.

data also were acquired at approximately g_x, g_z, and intermediate between g_y and g_z (data not shown). The values of T_1 and the widths of the distributions were similar for the four positions in the spectrum, which implies that anisotropy is not a major contributor to the widths of the distributions. One possibility is that the wide distributions may arise from distributions of the exchange interactions between irons in the cluster. Simulations of the CW spectra for the $[4Fe\text{-}4S]^{+}$ clusters in MftC at 20 K required linewidths of 34 to 44 G, and substantial g strain [14]. These linewidths are much larger than the low temperature linewidths of about 10 G for the $[2Fe\text{-}2S]^{+}$ cluster in PFL-AE [13] and much larger than the relaxation-determined linewidth which is much < 1 G at 20 K. Since ~98% of Fe has $I = 0$, there is no contribution to the linewidths from metal nuclear hyperfine splitting. The large linewidths for the $[4Fe\text{-}4S]^{+}$ clusters in MftC suggest substantial variations in the local environments of the clusters, which may also relate to the wide distributions in relaxation times. The wide distributions may be evidence for substantial mobility of the clusters [3,4]. Further work on other $[4Fe\text{-}4S]^{+}$ clusters is needed to understand the linewidths and the insights about the spin systems that can be gained by analysis of the distributions.

3.5. Impact of signal-to-noise on calculations for distributions using UPEN

Low signal-to-noise causes uncertainties in calculations of probability distributions that can result in broadening of the distributions and decreased values of β, that are not necessarily indicative of distinguishable contributions to relaxation. The data that were analyzed in the study (except as noted for HydF at 15, 50, and 60 K and for V $(cat)_3^{2-}$ at 160 and 180 K) had signal-to-noise > 100. To test whether distribution widths were limited by low signal-to-noise, running-average smoothing was applied to representative data sets. For example, for $[2Fe\text{-}2S]^{+}$ in PFL-AE at 60 K application of a 5-point running average smooth of the original data prior to analysis with UPEN caused only modest sharpening of the distribution (Fig. 7). When smoothing was applied to the inversion recovery data for HydF at 60 K (signal-to-

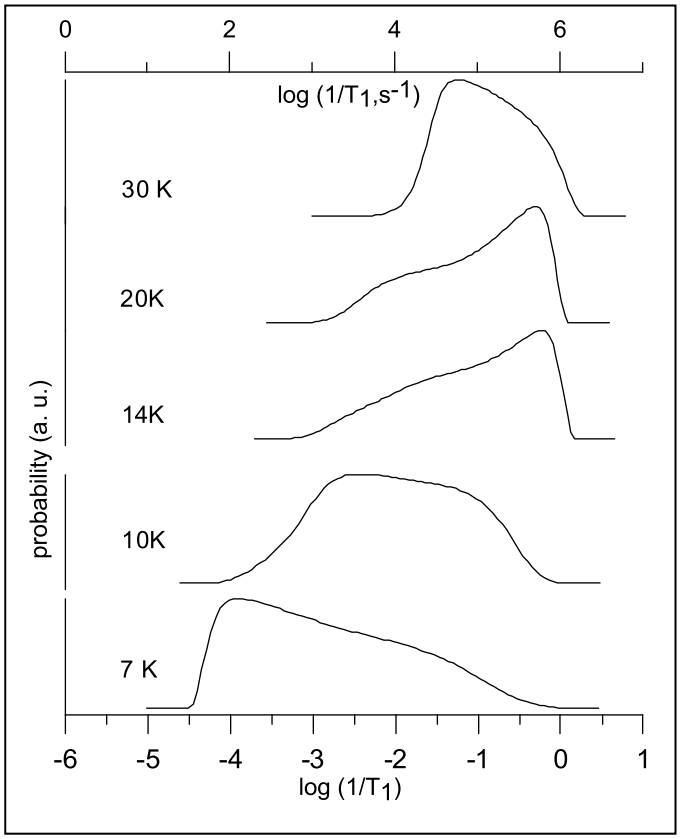

Fig. 11. Examples of the probability distributions for $1/T_1$ of $[4Fe\text{-}4S]^{+}$ in MftC calculated with UPEN (Eq. 5) at selected temperatures. The lower x axis is based on T_1 in μs for which $\log(1/T_1) = 0$ corresponds to $T_1 = 1$ μs. The upper axis is based on T_1 in s, which are the units for the y axis of Fig. 10.

noise = 42) the UPEN distribution (Fig. 9) suggested multiple components. However, for the HydF data at lower temperatures evidence was not found for multiple components and smoothing of the inversion recovery curves had negligible impact on the calculated distributions. This observation suggests caution in interpreting sharpening of distributions that is observed only for smoothed data.

3.6. Comparison with prior studies of EPR relaxation distributions

Although stretched exponentials have been used extensively to analyze nuclear spin relaxation rate distributions in solid state NMR [19–21], there has been relatively little use of this method to analyze T_1 in EPR [22–26]. Earle et al. concluded that the heterogeneity of the dynamics for nitroxide radicals in glassy *o*-terphenyl did not fit the distributions that are modeled with a stretched exponential [38]. Pfenninger et al. used stretched exponentials (Eq. (3)) to fit saturation recovery data for the dinuclear copper site of nitrous oxide reductase [22]. The T^n dependence for $1/T_1$ had $n = 3.3$ or 3.9 for the long and short components of a two exponential fit (Eq. (2)), respectively, or $n = 5$ for a stretched exponential fit (Eq. (3)). There was no interpretation of the difference in values of n. Magon et al. used a stretched exponential (Eq. (3)) to fit inversion recovery curves for doped polyaniline [39]. The value of β was about 0.7 in the temperature range of 7 to 40 K. Durny et al. used a stretched exponential to analyze inversion recovery data for amorphous hydrogenated silicon [40]. The value of β increased from about 0.3 at 10 K to about 1.0 at room temperature. Values of T_1 and β increased when samples were annealed or light soaked. Either light soaking or annealing may lower local spin concentrations, so these observations suggest that lower values of β may reflect increased contributions from spin diffusion, similar to what was observed for $V(cat)_3^{2-}$. Goslar et al. obtained T_1 for S_3^- ions in the sodalite cages of ultramarine blue using stretched exponentials [41]. The value of β increased from about 0.3 at 4.2 K to 0.8 at 50 K. The increasing values of β with temperature were attributed to increasing rates of reorientation of the ions that average the 12 inequivalent environments in the lattice.

Analysis with UPEN has the advantage over a stretched exponential that it provides insight into the nature of the distribution. It distinguishes between cases where there are distinguishable contributions to the distribution from ones with broad distributions. However, as with any analysis of distributions, results are more reliable when the signal-to-noise is relatively high.

4. Conclusions

When inversion recovery curves are fit as the sum of two exponentials (Eq. (2)) there is substantially more scatter in the values of T_1 than is observed for single exponential fits to the same data, which adds uncertainty to analysis of temperature dependence. Furthermore, unless a physical model predicts two components, analysis as a distribution is preferable.

For the data analyzed in this study, fits with a stretched exponential were statistically indistinguishable from the sum of two exponentials, and both were substantially better than with a single exponential. The stretched exponential has the advantage that the possibility of a distribution is explicitly acknowledged. When the value of the stretch parameter β is temperature dependent, use of the average T_1 value calculated using Eq. (4) is preferable for analyzing the temperature dependence of the relaxation. Low signal-to-noise can cause uncertainty in defining distributions and result in low values of β. Stretched exponentials are convenient tools for fitting distributions of exponentials. However, unless there is a physical model for the distribution, fitting the data with a model-free distribution as is done in UPEN is needed to interpret trends in β.

For the systems studied here the geometric mean of T_1 calculated with UPEN is similar to the average value calculated from the stretch exponential fit (Eq. 4), indicating that the two analyses are consistent. UPEN is useful for characterizing distributions, for recognizing changes in the shapes of distributions as a function of temperature, and for interpreting changes in the stretch parameter β. Each of these cases was demonstrated in data shown in this paper. If there are two components with distinguishable relaxation rates, this can be revealed by the UPEN distributions, without an initial assumption of two components, and the two components can be quantitated. Decreasing values of β at lower temperatures were observed for samples for which UPEN analysis showed significant contributions to the inversion recovery curves from spectral diffusion as for $V(cat)_3^{2-}$ or the detection of an additional faster relaxing species as was observed for PFL-AE. These observations related to analysis of distributions of rates may also be relevant to other kinetic systems.

For $V(cat)_3^{2-}$ modeling of the temperature dependence of the relaxation rates indicated an energy of the local mode of 305 cm^{-1} that is in a range that is expected for metal-ligand vibrations. For the $[2Fe\text{-}2S]^+$ in PFL-AE the distribution of relaxation times at temperature below about 30 K revealed contributions from a more rapidly relaxing $[3Fe\text{-}4S]^+$ cluster, which was difficult to distinguish by other analyses. For the $[4F3\text{-}4S]^+$ clusters in MftC the wide distributions in relaxation times may reflect large variations in electronic structure and protein mobility.

Abbreviations

CW	continuous wave
EPR	electron paramagnetic resonance
HydF	hydrogenase maturase F
MftC	S-adenosylmethionine protein mycofactocin maturase
NMR	nuclear magnetic resonance
PFL-AE	pyruvate formate lyase activating enzyme
UPEN	model free distribution of exponentials designated as uniform penalty inversion of multiexponential decay data

Acknowledgments

Partial financial support of this work from National Science Foundation (USA) AIP grant CHE-1836537 (SSE), National Institutes of Health grant CA177744 (SSE and GRE), and National Institutes of Health (USA) NIGMS grant 124002 (JAL) is gratefully acknowledged.

References

[1] S.S. Eaton, G.R. Eaton, Biol. Magn. Reson. 19 (2000) 29–154.
[2] W. Froncisz, J.S. Hyde, J. Chem. Phys. 73 (1980) 3123–3131.
[3] D.O. Hearshen, W.R. Hagen, R.H. Sands, H.J. Grande, H.L. Crespi, I.C. Gunsalus, W.R. Dunham, J. Magn. Reson. 69 (1986) 440–459.
[4] M. Sarewicz, M. Dutka, R. Pietras, A. Borek, A. Osyczka, Phys. Chem. Chem. Phys. 17 (2015) 25297–25308.
[5] B.J. Gaffney, H.J. Silverstone, Biol. Magn. Reson. 13 (1993) 1–57.
[6] G.C. Borgia, R.J.S. Brown, P. Fantazzini, J. Magn. Reson. 132 (1998) 65–77.
[7] G.C. Borgia, R.J.S. Brown, P. Fantazzini, J. Magn. Reson. 147 (2000) 273–285.
[8] S.S. Amin, K. Cryer, B. Zhang, S.K. Dutta, S.S. Eaton, O.P. Anderson, S.M. Miller, B.A. Reul, S.M. Brichard, D.C. Crans, Inorg. Chem. 39 (2000) 406–416.
[9] D.C. Crans, L. Yang, A. Haase, X. Yang, Met. Ions Life Sci. 18 (2018) 251–279.
[10] D.C. Crans, J.T. Koehn, S.M. Petry, C.M. Glover, A. Wijetunga, R. Kaur, A. Levina, P.A. Lay, Dalton Trans. 48 (2019) 6383–6395.
[11] C.-Y. Lin, T. Ngendahimana, G.R. Eaton, S.S. Eaton, J.M. Zadrozny, Chem. Sci. 10 (2019) 548–555.
[12] R.J. Usselman, A.J. Fielding, F.E. Frerman, G.R. Eaton, S.S. Eaton, Biochemistry 47 (2008) 92–100.
[13] E.M. Shepard, A.S. Byer, P. Aggarwal, J.N. Betz, A.G. Scott, K.A. Shisler, R.J. Usselman, G.R. Eaton, S.S. Eaton, J.B. Broderick, Biochemistry 56 (2017) 3234–3247.
[14] R. Ayikpoe, T. Ngendahimana, M. Langton, S. Bonitatibus, L.M. Walker, S.S. Eaton, G.R. Eaton, M. Eirini-Pandelia, S.J. Elliott, J.A. Latham, Biochemistry 58 (2019) 940–950.
[15] R.J.S. Brown, J. Magn. Reson. 82 (1989) 539–561.
[16] N.J. Clayden, B.D. Hesler, J. Magn. Reson. 98 (1982) 271–282.
[17] S.H. Koenig, R.D. Brown, Magn. Reson. Med. 1 (1984) 437–449.
[18] R.G. Rossing, M.B. Danforth, Biometrics 24 (1968) 117–134.

[19] M. Laviolette, M. Auger, S. Desilets, Macromolecules 32 (1999) 1602–1610.
[20] W.E. Kenyon, P.I. Day, C. Straley, J.F. Willemsen, SPE Formation Evaluation, September (1988), pp. 622–636.
[21] M. Peyron, G.K. Pierens, A.J. Lucas, L.D. Hall, R.C. Stewart, J. Magn. Reson. A 118 (1996) 214–220.
[22] S. Pfenninger, W.E. Antholine, M.E. Barr, J.S. Hyde, P.M.H. Kroneck, W.G. Zumft, Biophys. J. 69 (1995) 2761–2769.
[23] D. Stinghen, M. Atzori, C.M. Fernandes, R.R. Ribeiro, E.L. deSa, D.F. Back, S.O.K. Giese, D.L. Hughes, G.G. Nunes, E. Morra, M. Chiesa, R. Sessoli, J.F. Soares, Inorg. Chem. 57 (2018) 11393–11403.
[24] L. Tesi, E. Lucaccini, I. Cimatti, M. Perfetti, M. Mannini, M. Atzori, E. Morra, M. Chiesa, A. Caneschi, L. Sorace, R. Sessoli, Chem. Sci. 7 (2016) 2074–2083.
[25] M. Atzori, S. Benci, E. Morra, L. Tesi, M. Chiesa, R. Torre, L. Sorace, R. Sessoli, Inorg. Chem. 57 (2018) 731–740.
[26] C.-J. Yu, M.J. Graham, J.M. Zadrozny, J. Niklas, M.D. Krzyaniak, M.R. Wasielewski, O.G. Poluektov, D.E. Freedman, J. Amer. Chem. Soc. 138 (2016) 14678–14685.
[27] N. Stein, L. Mainali, J.S. Hyde, W.K. Subczynski, Appl. Magn. Reson. 50 (2019) 903–918.
[28] I.M. Brown, Electron spin echo studies of relaxation processes in molecular solids, in: L. Kevan, R.N. Schwartz (Eds.), Time Domain Electron Spin Resonance, John Wiley, New York, 1979, pp. 195–229.
[29] K.M. Salikhov, Y.D. Tsvetkov, Electron spin-echo studies of interactions in solids, in: L. Kevan, R.N. Schwartz (Eds.), Time Domain Electron Spin Resonance, Wiley, New York, 1979, pp. 232–277.
[30] H. Chen, A.G. Maryasov, O.Y. Rogozhnikova, D.V. Trukhin, V.M. Tormyshev, M.K. Bowman, Phys. Chem. Chem. Phys. 18 (2016) 24954–24965.
[31] J.R. Harbridge, S.S. Eaton, G.R. Eaton, J. Phys. Chem. A 107 (2003) 598–610.
[32] M. Atzori, L. Tesi, E. Morra, M. Chiesa, L. Sorace, R. Sessoli, J. Amer. Chem. Soc. 138 (2016) 2154–b2157.
[33] M. Atzori, E. Morra, L. Tesi, A. Albino, M. Chiesa, L. Sorace, R. Sessoli, J. Amer. Chem. Soc. 138 (2016) 11234–11244.
[34] V. Kathirvelu, G.R. Eaton, S.S. Eaton, Appl. Magn. Reson. 37 (2010) 649–656.
[35] L. Yong, J. Harbridge, R.W. Quine, G.A. Rinard, S.S. Eaton, G.R. Eaton, C. Mailer, E. Barth, H.J. Halpern, J. Magn. Reson. 152 (2001) 156–161.
[36] K.E. Lawson, Spectrochim. Acta 17 (1961) 247–258.
[37] S.J. Swamy, A.D. Reddy, K. Bhaskar, Indian J. Chem. 40A (2001) 1166–1171.
[38] K.A. Earle, J.K. Moscicki, A. Polimeno, J.H. Freed, J. Chem. Phys. 106 (1997) 9996–10015.
[39] C.J. Magon, R.R. deSouza, A.J. Costa-Filho, E.A. Vidoto, R.M. Faria, O.R. Nascimento, J. Chem. Phys. 112 (2000) 2958–2966.
[40] R. Durny, S. Yamasaki, J. Isoya, A. Matsuda, K. Tanaka, J. Noncryst. Solids 164 - 166 (1993) 223–226.
[41] J. Goslar, S. Lijewski, S.K. Hoffmann, A. Jankowska, S. Kowalak, J. Chem. Phys. 130 (2009) 204504.